APPENDIX-I

A1.1Materials and Methods

All the reagents and solvents were received from the commercial source and used without further purification. The tetrabutylammonium salts used for anion screening experiments were purchased from Sigma- Aldrich®. The reactants, metal salts and solvents were purchased from Sigma- Aldrich®, Merck and HiMedia laboratory products. Milli-Q ultra-pure water with a resistivity of above 18.25 MΩ cm was used throughout all the experiments. Laboratory prepared fluoride contaminated water samples are made by dissolving known amounts of NaF in tape water.

Infrared spectra were recorded with a Perkin Elmer Frontier MIRFIR spectrometer. ^{1}H NMR spectra (400 MHz) and ^{13}C NMR spectra (101 MHz) were recorded on a JEOL ECS-400 NMR spectrophotometer in $CDCl_3$ at room temperature and the chemical shifts are reported in parts per million (ppm) downfield of Me_4Si (TMS) as internal standard. UV–Vis experiments were performed with Shimadzu UV-2600i spectrophotometer. The fluorescence measurements were performed in Hitachi F-2700 fluorescent spectrometer whereas Time Dependent photoluminescent (TRPL) analyses were studied using FLS1000, Edinburgh fluorescent spectrometer. The UV–Visible and fluorescence spectra were recorded using standard 3.5 mL quartz cuvette with 10 mm path length. The UV-Vis and fluorescence titrations were carried out with the respective probe molecules solution (either in DMSO or water) by adding known quantities of concentrated solution of the organic/inorganic anion salts in DMSO/water solution. Electron Spin Resonance (ESR) Spectra were recorded in JEOL, JES-FA200 spectrometer. The X-band (9.44 Hz) ESR spectra were recorded in frozen aqueous DMSO solution. Cyclic voltametric studies were also performed using Auto-lab potentiostate in a standard three electrode system (working electrode: glassy carbon, reference electrode: Ag/AgCl and auxiliary electrode: Pt wire) and tetrabutylammonium perchlorate solution was used as supporting electrolyte.

Kohn-Sham density functional theory (DFT), Time dependent DFT (TDDFT) and natural bond orbital (NBO) calculations as available on Gaussian 09 software is used to study the structural and electronic properties of the complexes. Unrestricted ωB97XD functional and 6-311+g (d,p) basis set is employed for calculation [1-3]. The Conductor-like Polarizable Continuum Model (CPCM) model is used as available in Gaussian 09 to account the DMSO environment around the species during calculation [4].

Binding constant determination:

The equilibrium constant of the interaction of the probe molecules with F^- ion is evaluated from the UV–Vis titration data by using Benesi-Hildebrand plot [5].

$$\frac{1}{\Delta A} = \frac{1}{S_t K b \Delta\varepsilon [L]} + \frac{1}{S_t b \Delta\varepsilon}$$

Where, ΔA: measured absorbance of the substrate in absence and presence of anion, S_t: total host concentration (M), [L]: the anion concentration (M), K: Binding constant (M^{-1}), Δε: Molar absorptivity of the host–guest solution and b: Path length.

Limit of Detection Calculation (LOD):

The LODs were calculated from the respective calibration curve obtained from UV-Visible, fluorescence and differential pulse voltammetry techniques by following the equation:

$$LOD = \frac{3.3\sigma}{S}$$

where σ represents the standard error of the intercept of the linearly fitted straight line and S is the slope over a fixed linear range [5].

Calculation of *g*-value

The magnetic properties of the complex were determined by taking the parameters obtained from EPR data by following the formula

$$g = \frac{h\nu}{\mu_B B}$$

Where, h is Planck's constant, ν is the frequency of the EPR measurement, μ_B is the Bohr magneton ($9.274009994\times10^{-24}$ J·T^{-1}) and B is the magnetic field strength at which resonance occurs [6].

Calculation of fluorescence quantum yield:

The quantum yield was calculated by considering Rhodamine B as reference by using the formulae shown below [7]:

$$\Phi_{fx} = \frac{\eta_x^2}{\eta_{Rhodamine\ B}^2} \frac{A_{Rhodamine\ B}}{A_x} \frac{F_x}{F_{Rhodamine}} \times \Phi_{f,Rhodamine\ B}$$

where, ϕ_{fx} is the Quantum yield; η_x is the refractive indices of sample; η_{RB} is the refractive indices of Rhodamine blue; A_x is the absorbance of sample; A_{RB} is the absorbance of Rhodamine blue; F_x is the integrated area of sample; $F_{xRhodamine\ B}$ = integrated area of Rhodamine B; $\phi_{f,rhodamine\ B}$ is the Quantum yield of Rhodamine blue; $\phi_{fRhodamine\ B}$ is taken as 0.94 in water and $\eta_{Rhodamine\ B}$ is taken as 1.33 in water.

A1.2. Reference

[1] Frisch, M. J., Trucks, G. W., Schlegel, H. B., Scuseria, G. E., Robb, M. A., Cheeseman, J. R., Scalmani, G., Barone, V., Petersson, G. A., Nakatsuji, H., Li, X., Caricato, M., Marenich, A. V., Bloino, J., Janesko, B. G., Gomperts, R., Mennucci, B., Hratchian, H. P., Ortiz, J. V., Izmaylov, A. F., Sonnenberg, J. L., Williams-Young, D., Ding, F., Lipparini, F., Egidi, F., Goings, J., Peng, B., Petrone, A., Henderson, T., Ranasinghe, D., Zakrzewski, V. G., Gao, J., Rega, N., Zheng, G., Liang, W., Hada, M., Ehara, M., Toyota, K., Fukuda, R., Hasegawa, J., Ishida, M., Nakajima, T., Honda, Y., Kitao, O., Nakai, H.; Vreven, T., Throssell, K., Montgomery, J. A., Jr., Peralta, J. E., Ogliaro, F., Bearpark, M. J., Heyd, J. J., Brothers, E. N., Kudin, K. N., Staroverov, V. N., Keith, T. A., Kobayashi, R., Normand, J., Raghavachari, K., Rendell, A. P., Burant, J. C., Iyengar, S. S., Tomasi, J., Cossi, M., Millam, J. M.; Klene, M., Adamo, C., Cammi, R., Ochterski, J. W., Martin, R. L., Morokuma, K., Farkas, O.; Foresman, J. B., and Fox, D. J. Gaussian, Inc., Wallingford CT, 2016.

[2] Davidson, E. R. Computational transition metal chemistry. *Chemical reviews*, 100(2):351-352, 2000.

[3] Laurent, A. D., Adamo, C., and Jacquemin, D. Dye chemistry with time-dependent density functional theory, *Physical Chemistry Chemical Physics*, 6: 14334-14356, 2014.

[4] Cossi, M., Scalmani, G., Rega, N., and Barone, V. New developments in the polarizable continuum model for quantum mechanical and classical calculations on molecules in solution. *Journal of Chemical Physics*, 117: 43-54, 2004.

[5] Armbruster, D. A., and Pry, T. Limit of blank, limit of detection and limit of quantitation. *The clinical biochemist reviews*, 29(1):S49, 2008.

[6] Garribba, E., and Micera, G. The determination of the geometry of Cu (II) complexes: an EPR spectroscopy experiment. Journal of chemical education, 83:1229-1232, 2006

[7] Brouwer, A. M. Standards for photoluminescence quantum yield measurements in solution. *Pure and Applied Chemistry* 83(12):2213-2228, 2011.

APPENDIX-II

A2. Spectroscopic and Crystallographic data

A2.1. Spectroscopic Data

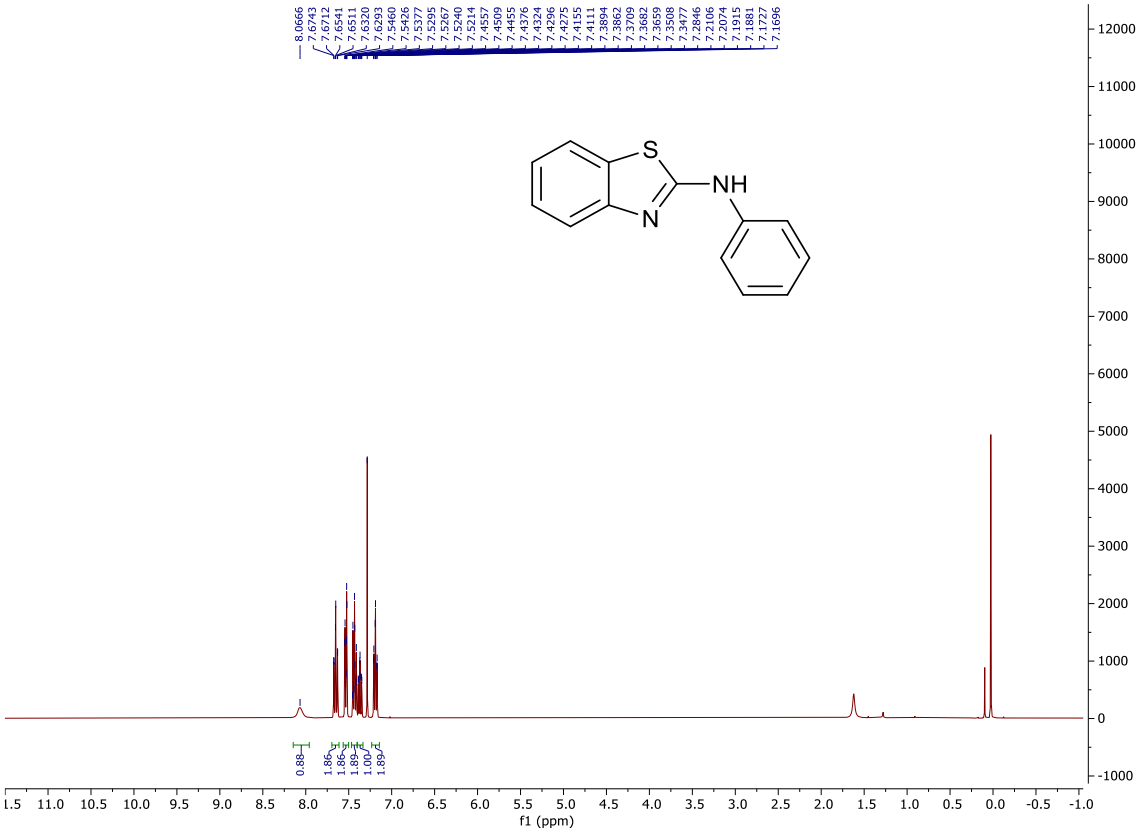

Figure A2.1: ^{1}H NMR spectrum of **R** in $CDCl_3$ solution.

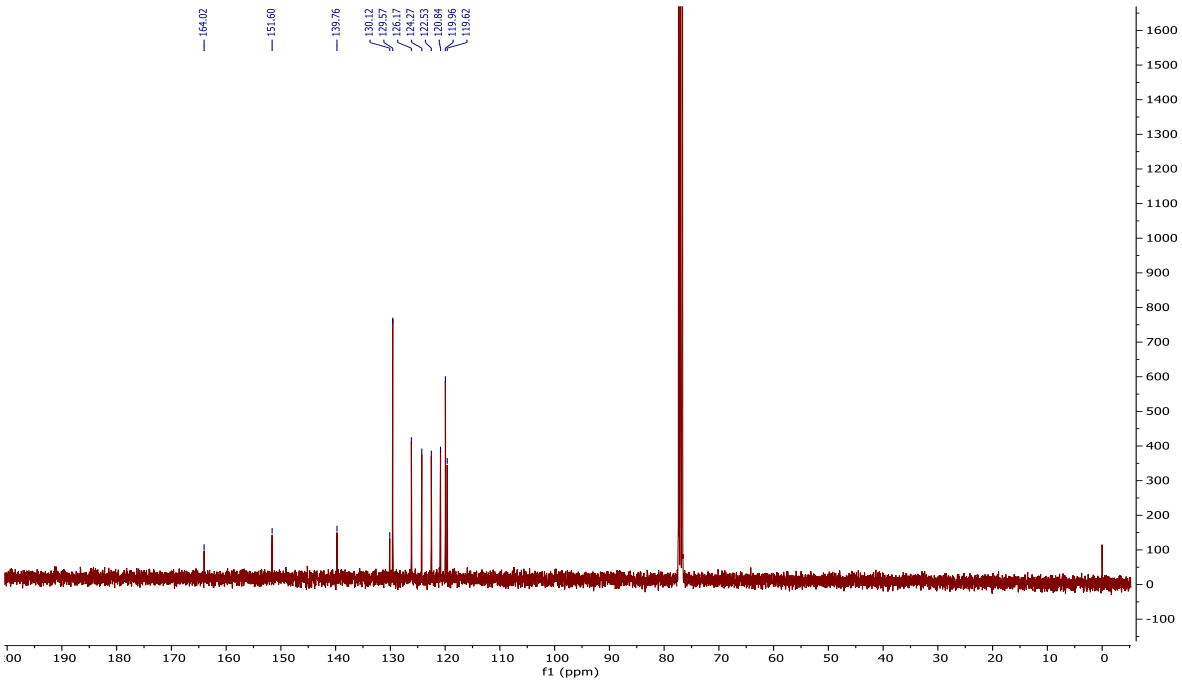

Figure A2.2: ^{13}C NMR spectrum of **R** in $CDCl_3$ solution.

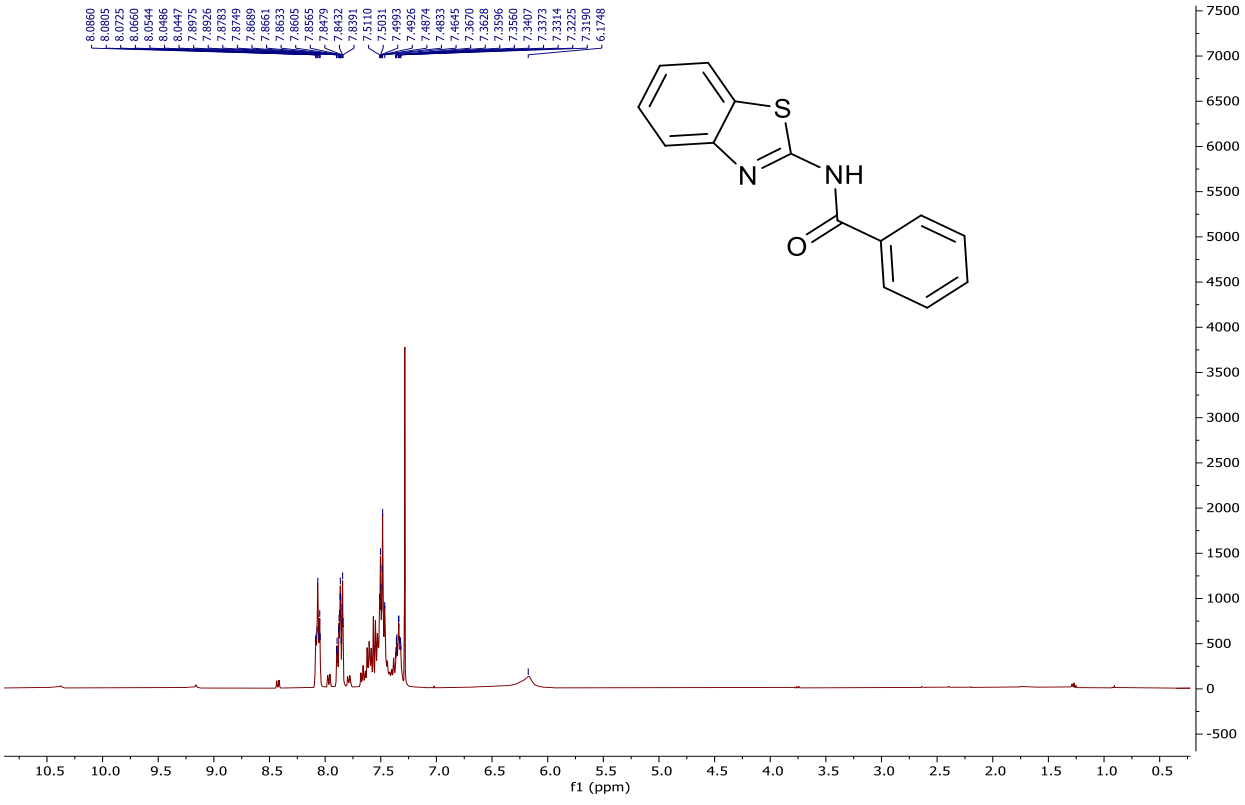

Figure A2.3: ^{1}H NMR spectrum of **P** in $CDCl_3$ solution.

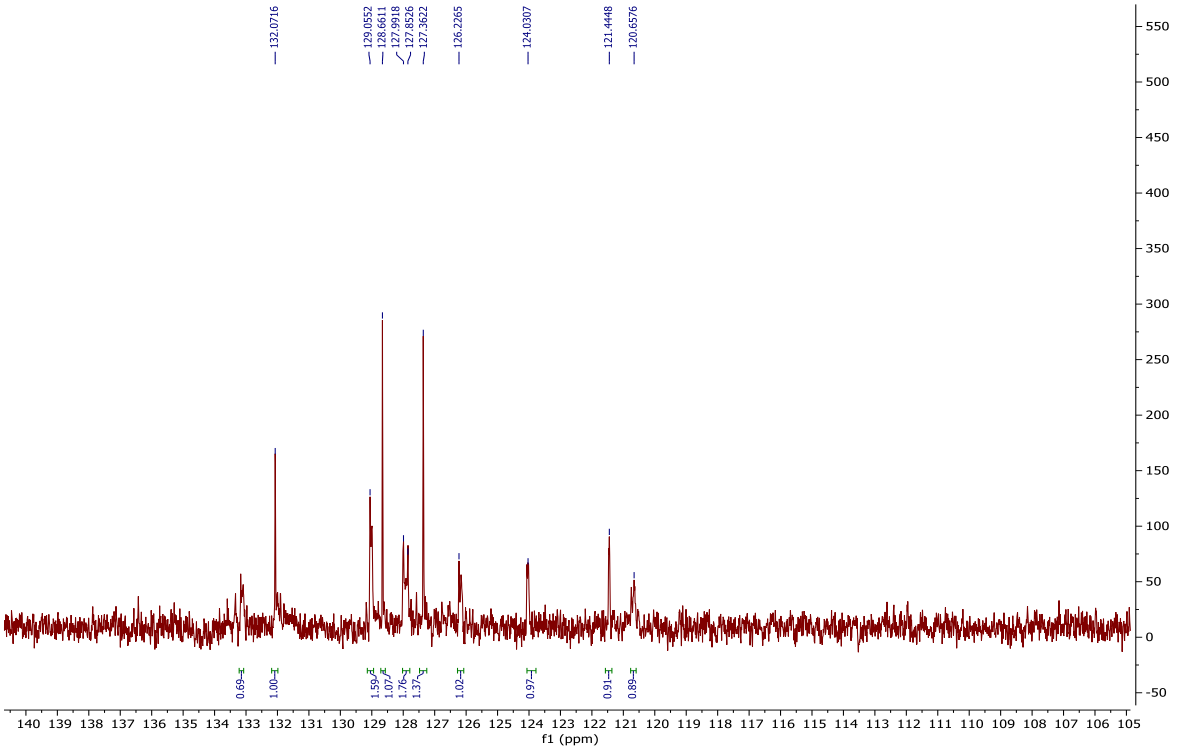

Figure A2.4: ^{13}C NMR spectrum of **P** in $CDCl_3$ solution.

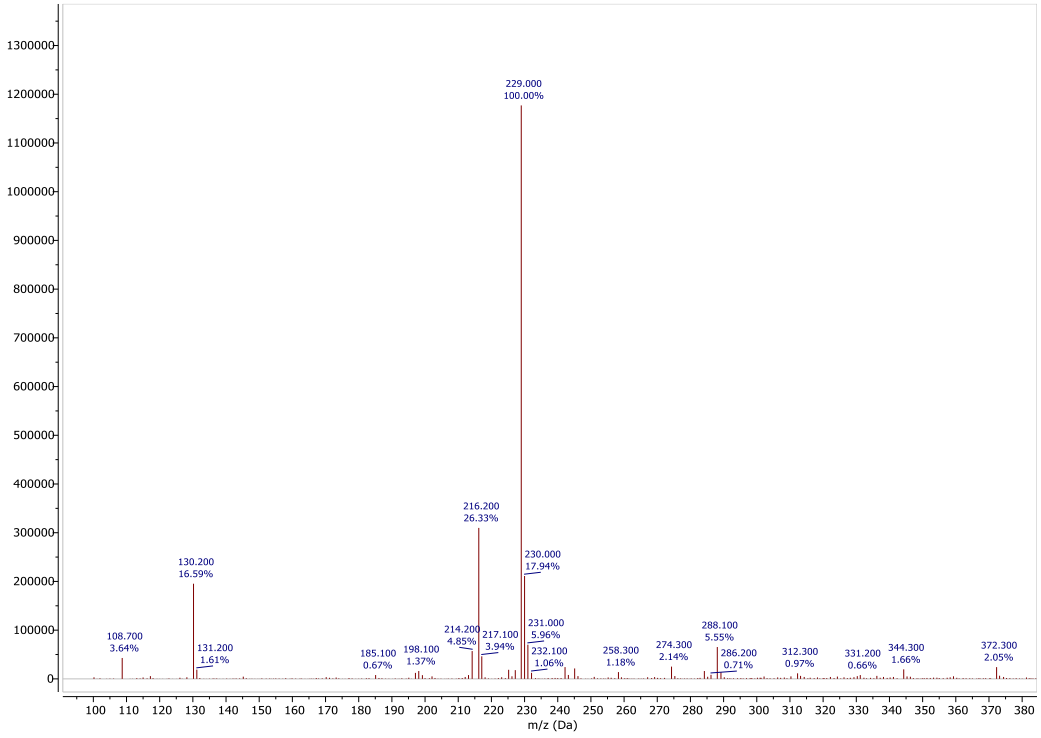

Figure A2.5: LCMS data of **R**.

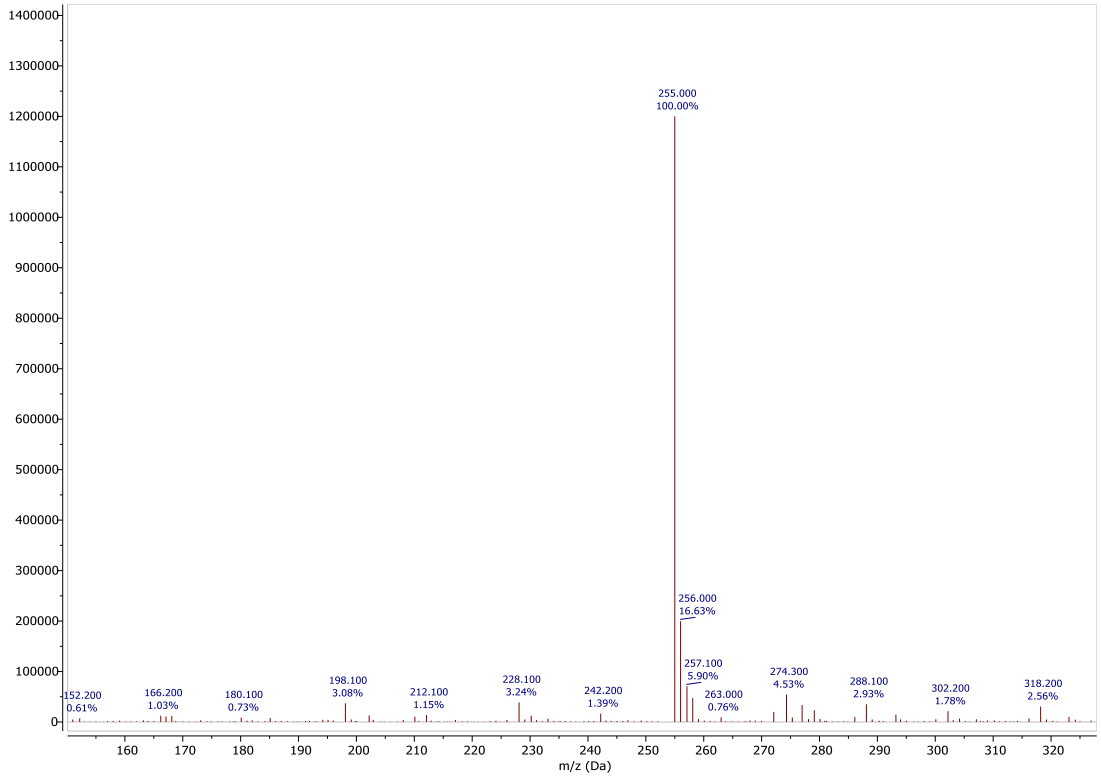

Figure A2.6: LCMS data of **P**.

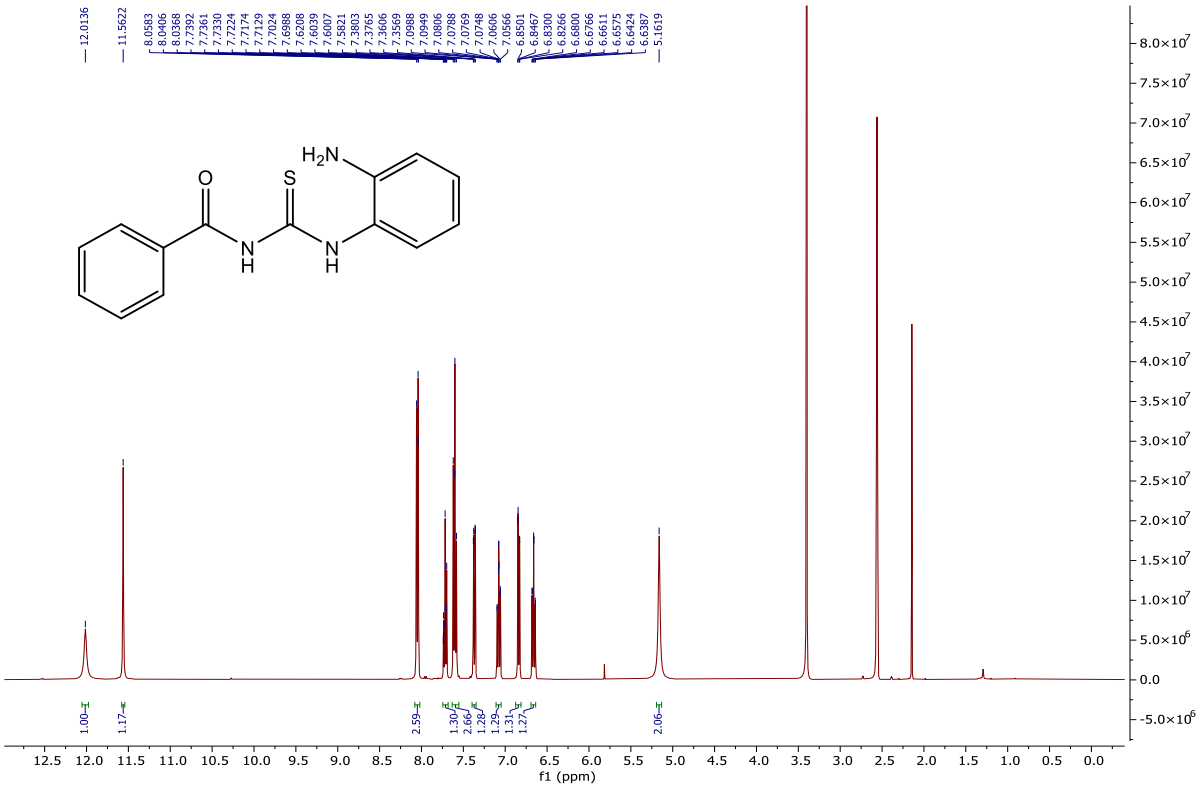

Figure A2.7: ^{1}H NMR spectrum of **B1** (DMSO-d_6, 298K)

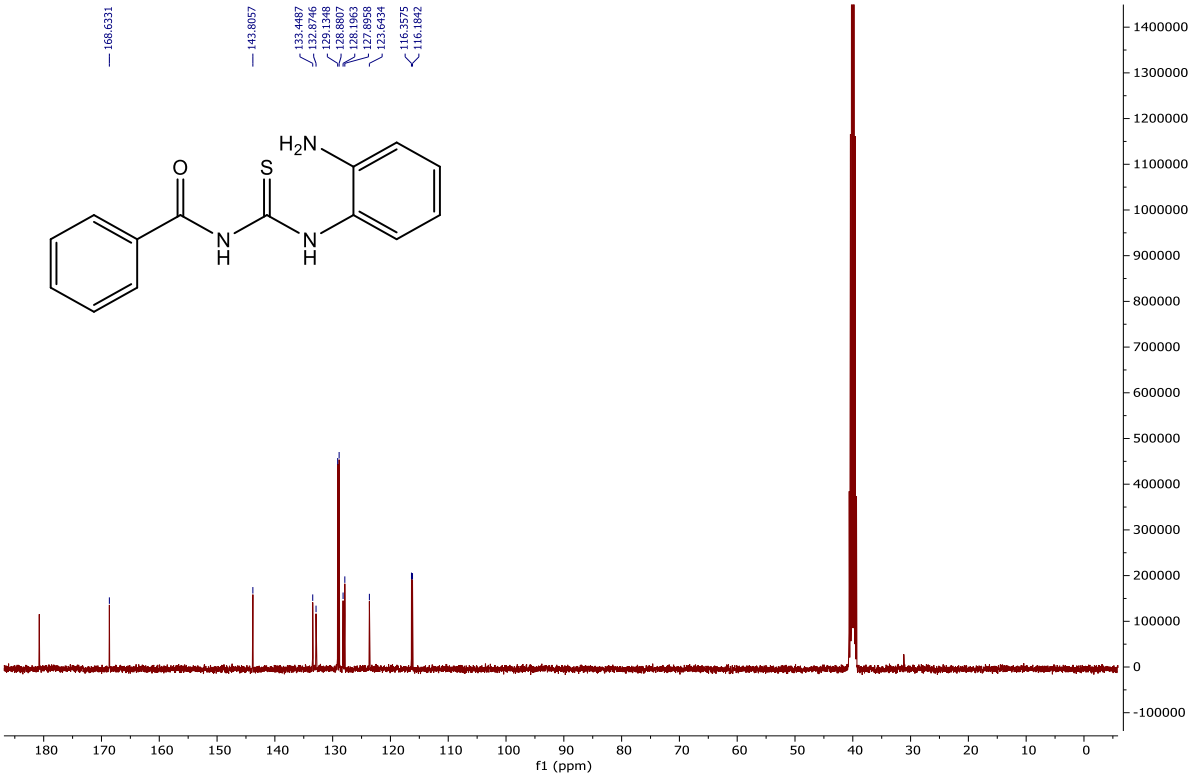

Figure A2.8: ^{13}C NMR spectrum of **B1** (DMSO-d_6, 298K)

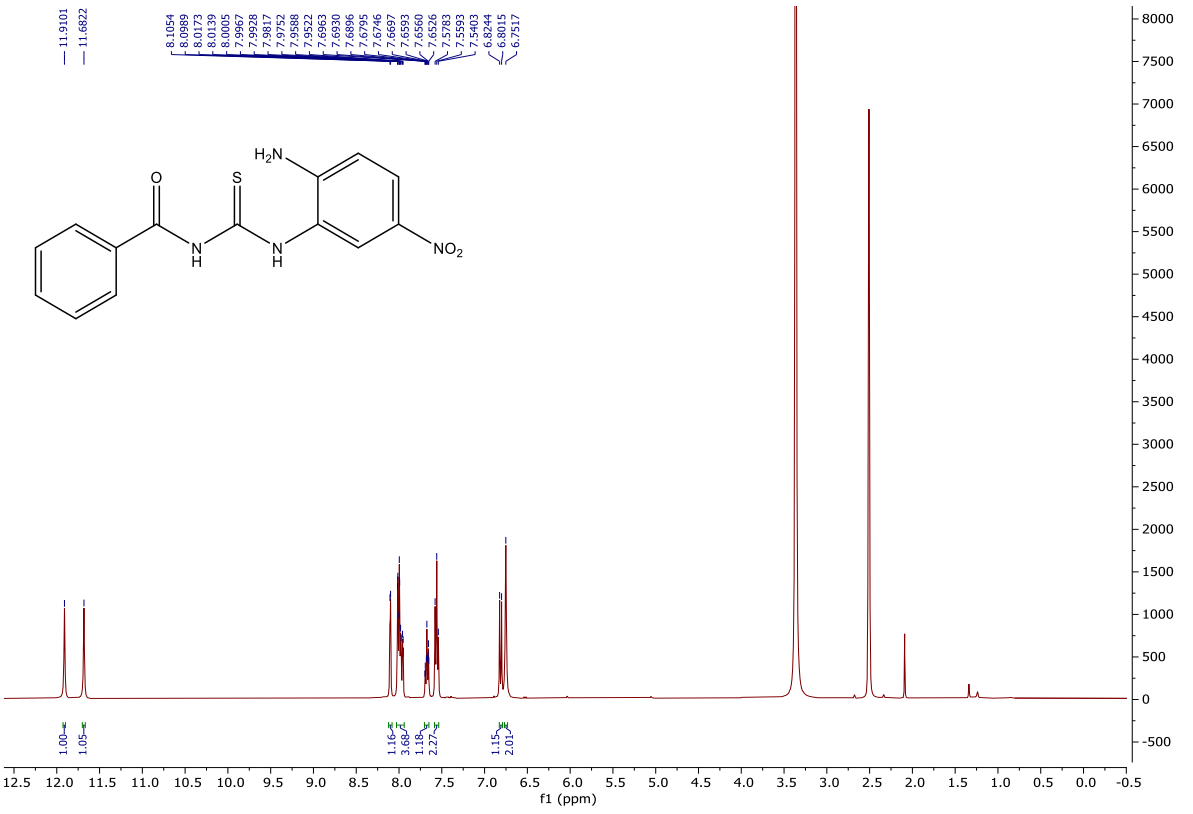

Figure A2.9: ^{1}H NMR spectrum of **B2** (DMSO-d_6, 298K)

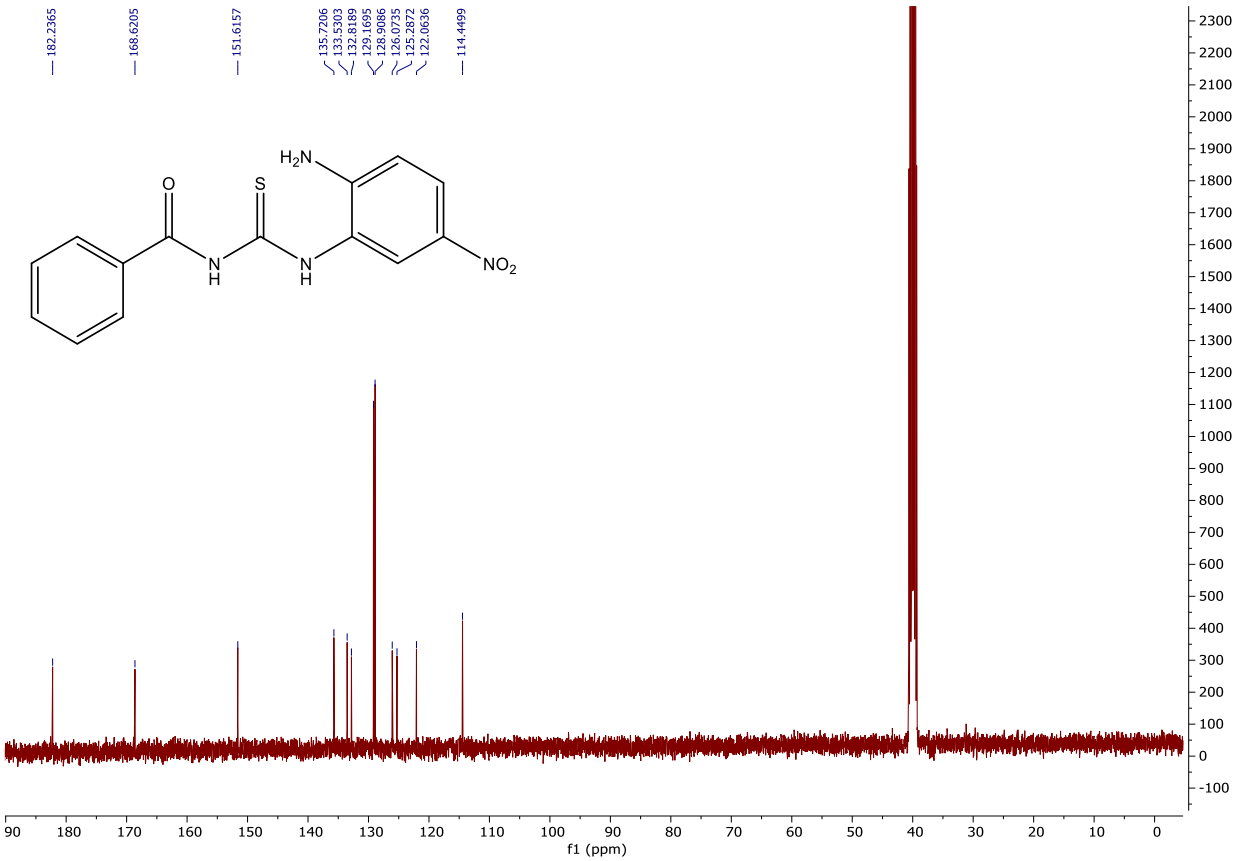

Figure A2.10: ^{13}C NMR spectrum of **B2** (DMSO-d_6, 298K)

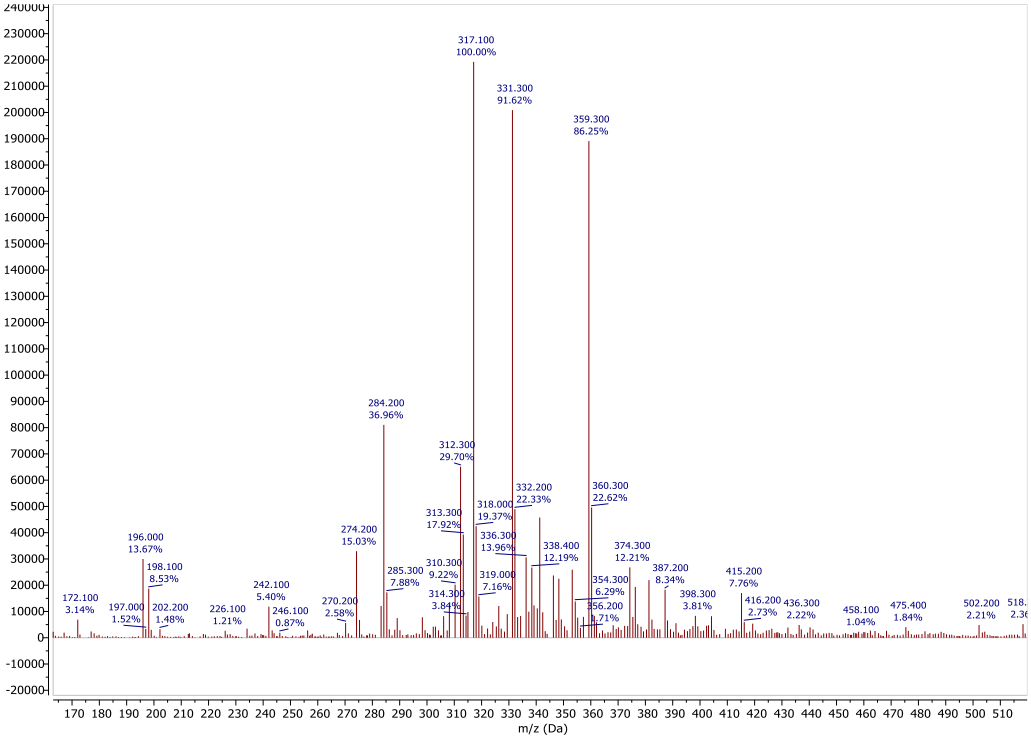

Figure A2.1111: LCMS data of **B2**.

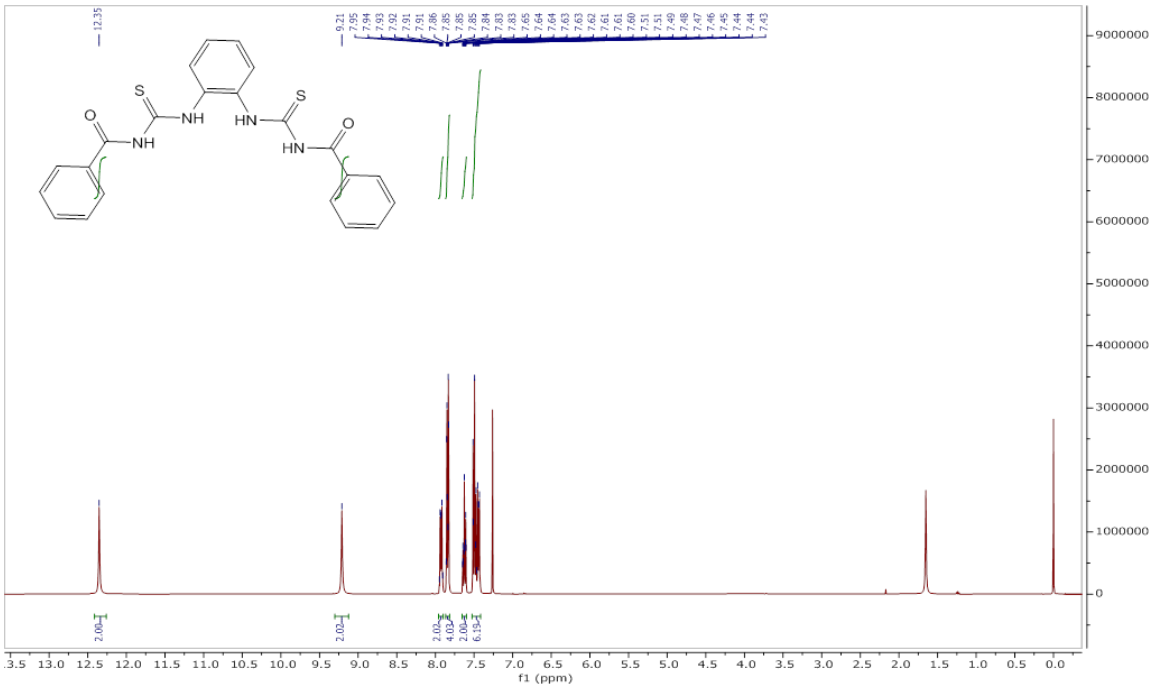

Figure A2.12: ^{1}H NMR spectrum of **S1** in $CDCl_3$ at 298K.

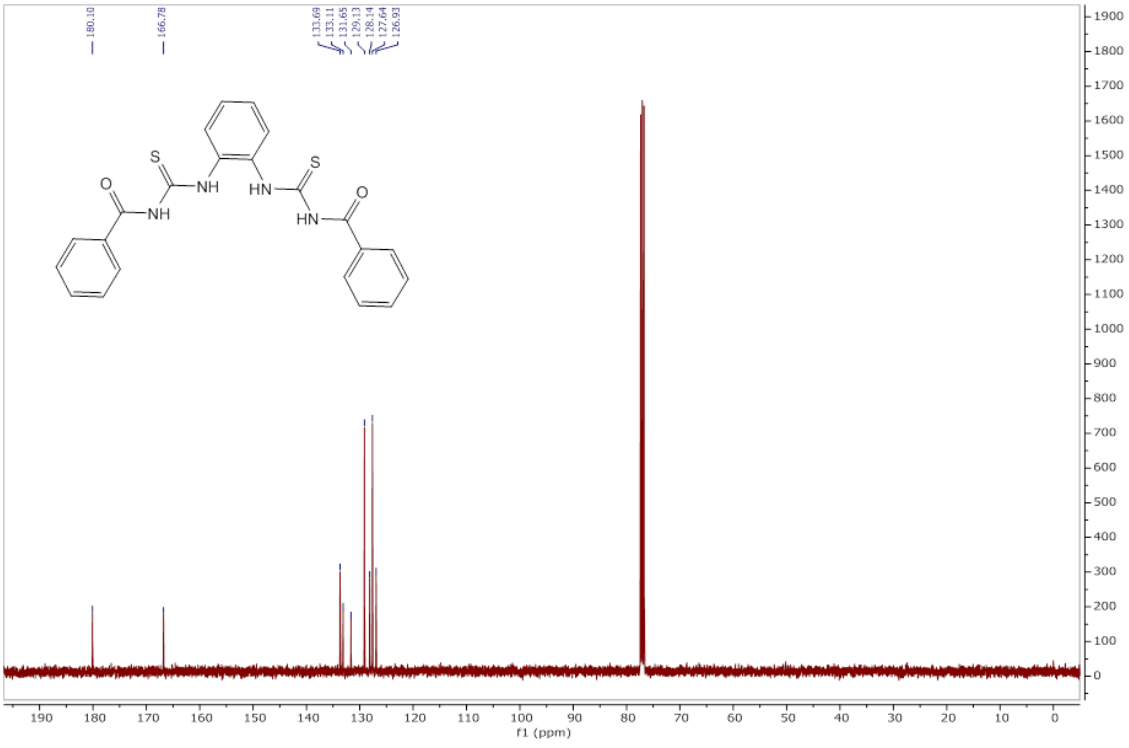

Figure A2.13: ^{13}C NMR spectrum of **S1** in $CDCl_3$ at 298K.

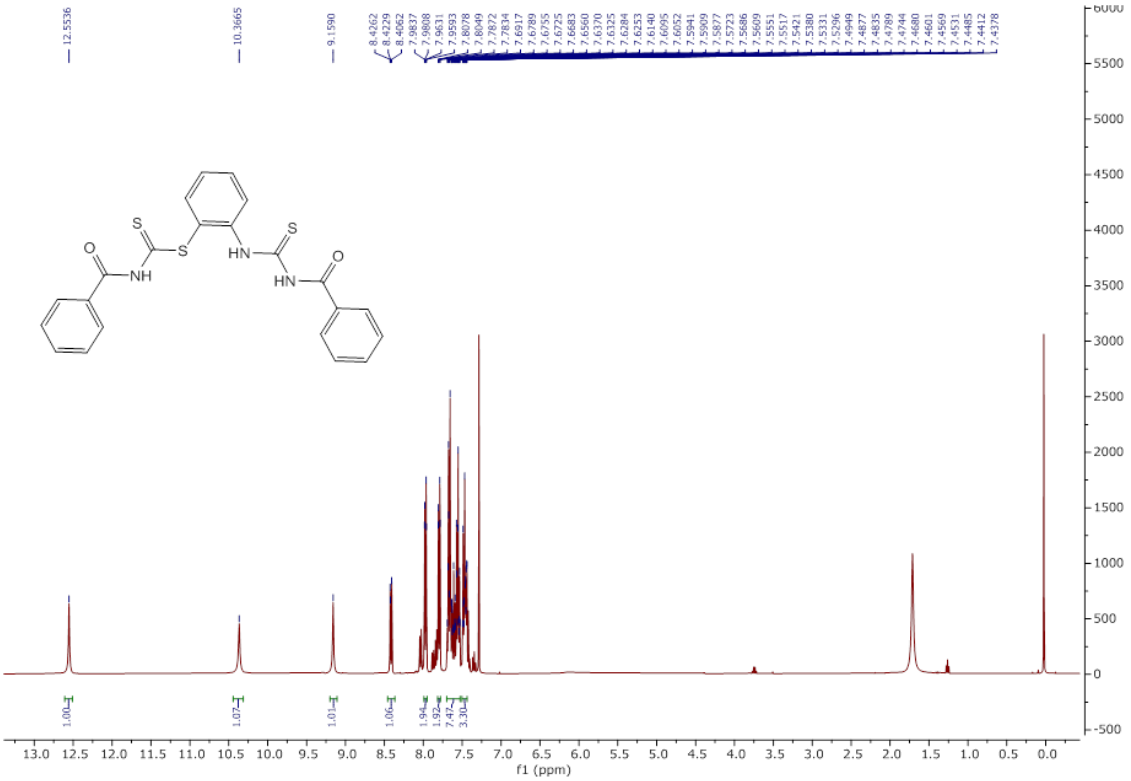

Figure A2.14: ^{1}H NMR spectrum of **S2** in $CDCl_3$ at 298K.

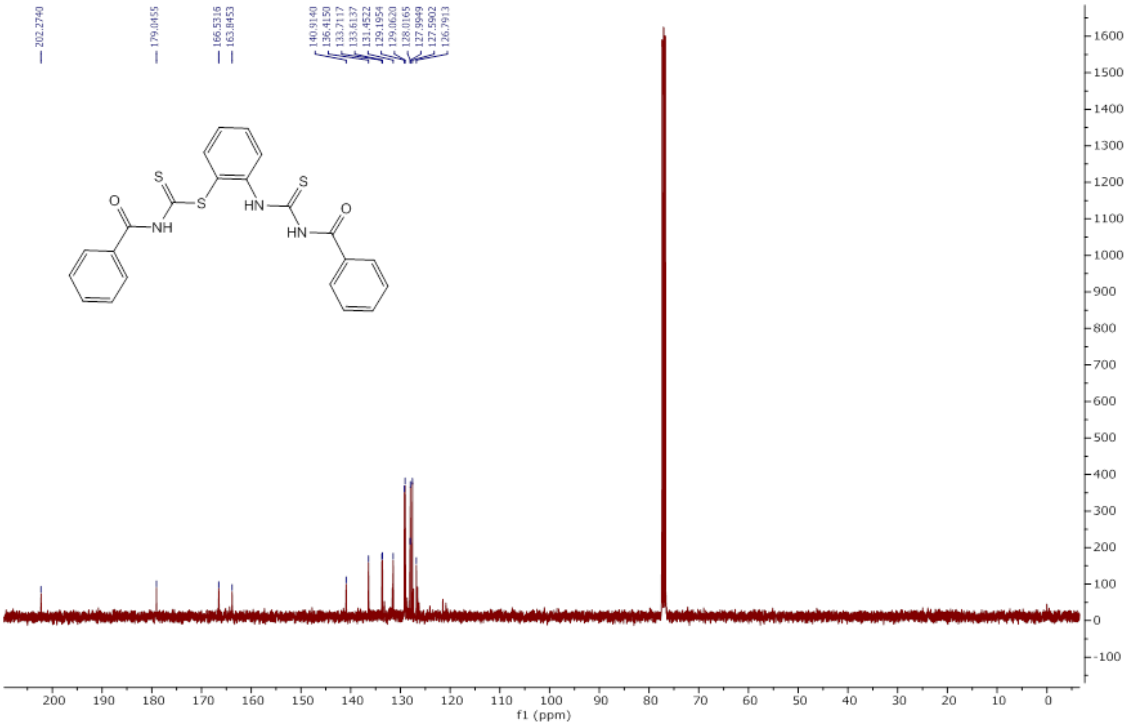

Figure A2.15: ^{13}C NMR spectrum of **S2** in $CDCl_3$ at 298K.

A2.2. Crystallographic Data

Compound Name	**R**	**P**	**B1**
Chemical formula	$C_{13}H_{10}N_2S$	$C_{14}H_{10}N_2OS$	$C_{10}H_{14}N_2O_2S$
M_r	226.29	254.26	201.31
Crystal system	Triclinic	Monoclinic	Triclinic
Space group	$P\bar{1}$	P21/n	$P\bar{1}$
Temperature (K)	296	296	296
a (Å)	4.0079(6)	5.9173(14)	9.8482(17)
b (Å)	10.9381(15)	16.910(4)	10.4134(17)
c (Å)	12.4755(18)	11.956(3)	13.956(2)
α (°)	97.354(4)	90	69.183(4)
β (°)	95.305(4)	102.238(6)	72.487(4)
γ (°)	92.045(4)	90	81.275(4)
V (Å^3)	539.46(13)	1169.1(5)	1274.2(4)
Z	4	4	16
Crystal density	2.786	0.427	4.197
Radiation type	Mo *K*α	Mo *K*α	Mo *K*α
μ (mm^{-1})	0.539	0.204	8.006
Diffractometer	Bruker *APEX*-II CCD diffractometer	Bruker *APEX*-II CCD diffractometer	Bruker *APEX*-II CCD diffractometer
Absorption correction	Multi-scan Bruker AXS *SADABS* program	Multi-scan Bruker AXS *SADABS* program	Multi-scan Bruker AXS *SADABS* program

No. of measured reflections	14498	16108	46120
No. of independent reflections	3087	3601	6209
No. of observed [$I > 2\sigma(I)$] reflections	2362	2411	4887
R_{int}	0.0684	0.09	0.0655
$(\sin \theta/\lambda)_{max}$ ($Å^{-1}$)	0.1605	0.1732	0.149
$R[F^2 > 2\sigma(F^2)]$	0.0463	0.0537	0.0493
$wR(F^2)$	0.116	0.129	0.1628
S	0.796	0.876	1.061
H-atom treatment	H atoms treated by a mixture of independent and constrained refinemen	H atoms treated by a mixture of independent and constrained refinement	H atoms treated by a mixture of independent and constrained refinement
$\Delta\rho_{max}$ (e $Å^{-3}$)	0.360	0.544	0.833
$\Delta\rho_{min}$ (e $Å^{-3}$)	-0.413	-0.625	−0.753
CCDC Number	2294780	2294781	-

Table A2.1: Crystallographic parameters of the crystal structures of probe molecule **R**, **P** and **B1**.

Compound Name	**Form 1_S1**	**Form 2_S1**	**S2**
Chemical formula	$C_{22}H_{18}N_4O_2S_2$	$C_{22}H_{18}N_4O_2S_2$	$C_{22}H_{17}N_3O_2S_3$
M_r	434.52	434.52	451.57
Crystal system	Triclinic	Triclinic	Triclinic
space group	$P\bar{1}$	$P\bar{1}$	$P\bar{1}$
Temperature (K)	296	296	296
a (Å)	7.187 (3)	9.354 (3)	8.006 (7)
b (Å)	12.122 (5)	13.492 (4)	10.260 (9)
c (Å)	12.481 (5)	17.372 (5)	13.445 (11)
α (°)	77.861 (13)	81.088 (9)	90.317 (9)
β (°)	86.967 (14)	77.129 (9)	106.383 (8)
γ (°)	77.720 (13)	82.111 (9)	99.195 (9)
V (Å^3)	1038.7 (7)	2099.5 (10)	1044.4
Z	2	4	2
Crystal density	1.389	1.375	1.436
Radiation type	Mo *K*α	Mo *K*α	Mo *K*α
μ (mm^{-1})	0.28		0.38
Diffractometer	Bruker *APEX*-II CCD diffractometer	Bruker *APEX*-II CCD diffractometer	Bruker *APEX*-II CCD diffractometer
Absorption correction	Multi-scan Bruker AXS *SADABS* program	Multi-scan Bruker AXS *SADABS* program	Multi-scan Bruker AXS *SADABS* program
No. of measured reflections	30540	83494	30615

No. of independent reflections	6217	12147	5025
No. of observed [$I > 2\sigma(I)$] reflections	3459	4062	2424
R_{int}	0.084	0.214	0.125
$(\sin\theta/\lambda)_{max}$ (Å^{-1})	0.714	0.708	0.125
$R[F^2 > 2\sigma(F^2)]$	0.064	0.069	0.057
$wR(F^2)$	0.217	0.227	0.151
S	1.01	0.93	0.96
H-atom treatment	H atoms treated by a mixture of independent and constrained refinement	H atoms treated by a mixture of independent and constrained refinement	H atoms treated by a mixture of independent and constrained refinement
$\Delta\rho_{max}$ (e Å^{-3})	0.37	0.38	0.24
$\Delta\rho_{min}$ (e Å^{-3})	−0.42	−0.36	−0.28
CCDC Number	2313674	2313673	2313675

Table A2. 2: Crystallographic parameters of the crystal structures of probe molecule **S1** and **S2**.

List of Publications

In international refereed journals.

[1] **Mushahary, B. C**., Buragohain, R., Neog, S., Biswakarma, N., Thakuria, R., Das, R., and Mahanta, S. P. Transition metal complexation assisted stabilization of the deprotonated organic moiety: A strategy for colorimetric and electrochemical recognition of fluoride ion in water medium with organic probe molecules. *Inorganic Chemistry Communications*, 112560, 2024.

[2] **Mushahary, B. C**., Biswakarma, N., Thakuria, R., Das, R., and Mahanta, S. P. In Situ Ni (II) Complexation Induced Deprotonation of Bis-Thiourea-Based Tweezers in DMSO–Water Medium: An Approach toward Recognition of Fluoride Ions in Water with Organic Probe Molecules. *ACS omega*, 9:29300−29309, 2024.

[3] Bharati, S. P., **Mushahary, B. C.**, Das, R., and Mahanta, S. P. Exploring in situ Ni (II) complexation of pyrrole-benzimidazole ligands towards colorimetric sensing of fluoride ion in aqueous medium. *Results in Chemistry*, *5*:100927, 2023.

[4] **Mushahary, B. C.**, Bora, D., and Goswami, C. Perylene Tetracarboxylate Dye Based Colorimetric and Fluorometric Sensor for ppb-Level Fluoride Detection in Water. *Dalton Trans*. [**Under communication**]

[5] **Mushahary, B. C.**, Bhuyan, M., Bora, D., and Das, R. Fluorescein Based Dual Optical Sensor for Highly Selective and Sensitive Fluoride Detection in 100 % water medium. *Chem. Comm*. [**Under communication**]

Book Chapter:

[1] Das, R., Bharati, S.P. and Mushahary, B.C. Designing chemosensors for fluoride detection. In Hashemi, A.R., editor, Research Trends in Applied Research, Volume 7, pages 49-75, ISBN: 9783964922366, Weser, 2021.

In Conferences (as abstract):

Oral Presentation

[1] **Mushahary, B. C.** and S. P. Mahanta, DETECTION OF FLOURIDE IN AQUEOUS MEDIUM USING *bis*-THIOUREA TWEEZERS via Ni^{2+} METAL COMPLEXATION, National seminar on "Sustainability, Medicine and Clear energy,"Tezpur University, Tezpur, 1st March, 2022.

[2] **Mushahary, B. C.** and S. P. Mahanta, Detection of Flouride in Aqueous Medium using Thiourea based probe via Ni^{2+} metal complexation, "National conference on "Advances in sustainable chemistry and material sciences", Bodoland University, Kokrajhar, 29th – 30th April, 2022.

[3] **Mushahary, B. C.** and S. P. Mahanta, In-Situ Ni(II) metal complexation induced deprotonation of Thiourea based probe enhances the colorimetric fluoride recognition in water, Internal national conference on "Recent advance in Mathematical, Physical and Chemical Sciences", MZU, Mizoram, 21st – 23rd February, 2024.

Poster Presentation

[1] **Mushahary, B. C.** and S. P. Mahanta, Benzothiazole based optical sensor for the detection of fluoride in aqueous medium, Internal national Symposium on "Emerging Trends in Chemical Sciences", NEHU, Shillong, 2nd – 4th March, 2023.